JOURNAL OF COMPUTATIONAL PHYSICS 46, 397–422 (1982)

Three-Dimensional Steady Stratified Flows: A Numerical Approach

W. K. STEVENS

Department of Mathematics,
504 Lake Hall, Northeastern University, Boston, Massachusetts 02115

AND

C. H. SU

Division of Applied Mathematics, Brown University, Providence, Rhode Island 02192

Received December 16, 1980; revised January 6, 1982

A multilayer model consisting of n homogeneous layers is used to describe the three-dimensional steady flow of a continuously stratified, incompressible fluid under the assumption of hydrostatic balance. For $n = 1$, one has the classical shallow water theory and the governing equations correspond to those for the steady two-dimensional flow of a compressible gas with γ, the ratio of specific heats, equal to 2. For $n > 1$, the equations form a nonlinear system of partial differential equations of order $2n$. For most practical stratified flow problems this system is neither totally hyperbolic or totally elliptic; i.e., it possesses both real and imaginary characteristics over the entire domain of interest. A numerical algorithm for this "mixed" case is proposed and calculations for a two-layer model are presented. Continuous solutions are shown to exist for sufficiently flat and smooth obstacles.

1. INTRODUCTION

This study concerns the steady three-dimensional continuous flow of an incompressible fluid. As an approximation to a continuously stratified and sheared fluid of finite depth, we consider a fluid composed of n homogeneous layers. Each layer is characterized by a thickness h_i, averaged horizontal velocity components $\bar{u}_i$ and $\bar{v}_i$, and a density ρ_i. The first three quantities h_i, $\bar{u}_i$, and $\bar{v}_i$ vary along streamlines while ρ_i remains constant due to the assumption of incompressibility. Such multilayer systems are of considerable practical interest in meteorology and oceanography due to the frequent occurrence of strong temperature inversions in the atmosphere and oceans. These inversion layers are dynamically similar to the interface between homogeneous layers. Thus this problem, of stratified flows around a three-dimensional mountain, has received considerable attention. For the most part, however, studies have been restricted to approaches in which the obstacle is taken to be a small perturbation of a plane surface; e.g. see Crapper [2] and Wong [10].

0021-9991/82/060397-26$02.00/0

Apparently the only exception is the theory of Drazin [3] which is valid asymptotically as the Froude number approaches zero. Recent experimental studies include those by Brighton [1], Hunt and Snyder [4], and Riley *et al.* [6]. Multilayer models in two dimensions are discussed in papers by Lee and Su [5] for continuous flows and by Su [8] for flows containing hydraulic jumps. While a multilayer model in two dimensions is governed by a system of nonlinear algebraic equations, however, multilayer models in three dimensions involve systems of nonlinear partial differential equations. We derive these equations under the assumptions of hydrostatic balance and a nonrotating frame of reference. Thus, valid applications of this model are subject to the following restrictions. First, due to the assumption of hydrostatics, our method applies only to motions in which vertical accelerations may be neglected; e.g., flows over barriers whose heights are much smaller than the horizontal dimensions of the problem. Secondly, we are further restricted to those flows for which the Coriolis force is negligible; e.g., small-scale atmospheric and oceanic phenomena such as airflow over individual mountain ranges and ocean flow around islands. Vertical averaging of the horizontal velocity components in each layer is also employed. The resulting set of equations consists of a mass conservation equation, vorticity equation and Bernouilli's theorem for each layer. In the degenerate case of one-layer flow, the equations are analogous to those governing certain two-dimensional flows in gas dynamics.

A general method of solution employing standard methods is available for the linearized n-layer model; however, for the sake of brevity we present here explicit solutions only for the two-layer model. Of interest primarily is the form of the linearized governing equations which is shown to suggest certain approximate methods of solution for the nonlinear equations, and secondly the linear solutions themselves which provide useful corroboration for the resulting nonlinear numerical solutions in the limit of infinitesimal obstacle height.

A numerical algorithm for the solution of the nonlinear equations is proposed, and calculations for the flow of a two-layer system over an obstacle, around a cylinder extending vertically through the total fluid depth, and around obstacles placed interior to the layers are presented. All the above solutions are shown to be continuous for moderate obstacle sizes.

2. Governing Equations

We divide the fluid of total depth H into n layers. Each layer has thickness $h_i(x, y)$, averaged horizontal velocity components $\bar{u}_i(x, y)$ and $\bar{v}_i(x, y)$ and density ρ_i. The capital letters H_i and U_i will be used for the corresponding physical quantities far upstream; i.e., $(U_i, H_i) = (\bar{u}_i, h_i)$ at $x = -\infty$ (note that $\bar{v}_i = 0$ at $x = -\infty$), and $H = \sum_{i=1}^{n} H_i$. The density ρ_i is constant in each layer. We denote by $h_0(x, y)$ an obstacle profile which vanishes as $|(x, y)| \to \infty$, and assume the flow in each layer to be steady, incompressible, two-dimensional, inviscid, and hydrostatic in a nonrotating frame of reference. A schematic of the fluid geometry is shown in Fig. 1.

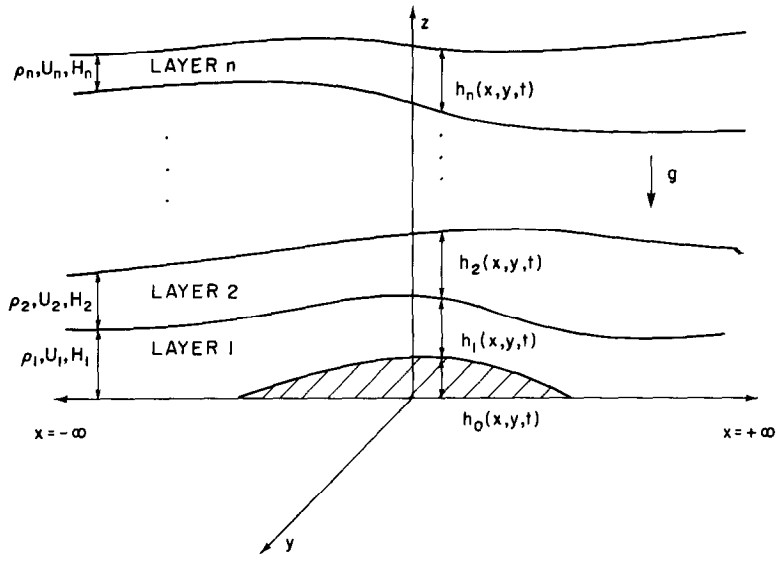

FIG. 1. Schematic of flow field.

The governing equations for each layer are mass continuity,

$$\frac{\partial h_i}{\partial t} + \frac{\partial}{\partial x}(h_i \bar{u}_i) + \frac{\partial}{\partial y}(h_i \bar{v}_i) = 0, \tag{1}$$

and momentum,

$$\frac{\partial \mathbf{q}_i}{\partial t} + (\mathbf{q}_i \cdot \nabla)\,\mathbf{q}_i + \frac{1}{\rho_i}\nabla p_i = 0, \qquad i = 1,\ldots, n, \tag{2}$$

where $\mathbf{q}_i = (\bar{u}_i, \bar{v}_i)$, $\nabla = (\partial/\partial x, \partial/\partial y)$, and the bars denote a vertical average in the ith layer; i.e.,

$$\bar{A}_i(x, y, t) = \frac{1}{h_i}\int_{z_{i-1}}^{z_i} A(x, y, z, t)\, dz.$$

In the above, $z_k(x, y, t)$ denotes the height of the fluid interface between the kth and $(k+1)$st layers,

$$z_k(x, y, t) = \sum_{j=0}^{k} h_j(x, y, t).$$

Using the hydrostatic relation and denoting the pressure at the top of the fluid as p_s, the pressure at a point within the ith layer may be written as

$$p_i(x, y, z, t) = p_s + g\sum_{j=i+1}^{n} \rho_j h_j + g\rho_i\left(\sum_{j=0}^{i} h_j - z\right),$$

where z is the height of the point above the reference level. Since the z dependence of $p_i(x, y, z, t)$ will drop out of (2) because of the ∇ operation, however, we shall hereafter denote p_i without explicit specification of independent variables as

$$p_i = p_s + g \sum_{j=i+1}^{n} \rho_j h_j + g\rho_i \sum_{j=0}^{i} h_j.$$

Equations (1) and (2), derived in Stevens [7], are the starting point of our study. Under the assumption of steady flow, they reduce to the following three basic equations in each layer:

$$\frac{\partial}{\partial x}(h_i \bar{u}_i) + \frac{\partial}{\partial y}(h_i \bar{v}_i) = 0, \tag{3}$$

$$\frac{1}{2}(\bar{u}_i^2 + \bar{v}_i^2) + p_i = B_i, \tag{4}$$

$$\nabla \mathbf{x} \mathbf{q}_i = 0, \tag{5}$$

where B_i is the Bernoulli constant

$$B_i = \frac{U_i^2}{2} + g \sum_{j=i+1}^{n} \frac{\rho_j}{\rho_i} H_j + g \sum_{j=0}^{i} H_j + \frac{P_s}{\rho_i}.$$

Note that the value of p_s far upstream is denoted here by P_s. Equations corresponding to (3) and (4) for multilayer models in two dimensions are given in Lee and Su [5] and Su [8]. Apparent from the form of (3) and (4) is the well-known fact that the theory for one-layer flow is analogous to that for steady two-dimensional flows in gas dynamics with γ, the ratio of specific heats, equal to 2.

For convenience, the bars over the averaged horizontal velocity components will be omitted in the remainder of this paper.

3. Linear Solutions

In this section we present the linear equations for the n-layer model with a free or rigid upper surface and outline a method for their solution. Explicit solutions are given for the two-layer model with a rigid upper surface.

a. *Free Upper Surface*

We expand u_i, v_i, and h_i in terms of a small parameter ε as

$$\mathbf{u}_i = (u_i, v_i) = \nabla(U_i x + \varepsilon \phi_i^{(1)} + \varepsilon^2 \phi_i^{(2)} + \cdots), \tag{6}$$

$$h_i = H_i + \varepsilon h_i^{(1)} + \varepsilon^2 h_i^{(2)} + \cdots, \tag{7}$$

where ϕ_i denotes the velocity potential in the ith layer and $h_0(x, y)$ specifies the

obstacle height. For flow over an obstacle the small parameter ε is given by the ratio of the width to the length (flowwise) of the obstacle. Substitution of (6) and (7) into (3) and (4) yields

$$H_i \nabla^2 \phi_i^{(1)} + U_i \frac{\partial}{\partial x} h_i^{(1)} = 0, \tag{8}$$

$$U_i \frac{\partial \phi_i^{(1)}}{\partial x} + g \sum_{j=i+1}^{n} \frac{\rho_j}{\rho_i} h_j^{(1)} + g \sum_{j=0}^{i} h_j^{(1)} = 0, \tag{9}$$

where we have used the free upper surface condition $p_s =$ constant and ignored $O(\varepsilon^2)$ terms.

As this system of $2n$ equations for the velocity potentials and layer thicknesses may be solved using standard methods, we shall give only a brief sketch of the procedure:

(i) Eliminate the layer thickness terms to obtain a system of n equations for the n velocity potentials.

(ii) Assume solutions of the form $\phi_i(x, y) = \psi_i(k_1, k_2)\, e^{i(k_1 x + k_2 y)}$; i.e., "plane wave" solutions, to obtain $k_1/k_2 = \pm\alpha_i$, $i = 1, 2, \ldots, n$, expressing the values of k_1/k_2 corresponding to nontrivial solutions. Here $1/\alpha_i$ gives the slope of the ith characteristic for real α_i.

(iii) The solution is then obtained by applying suitable boundary conditions. These consist of a condition at the obstacle, if necessary (see below), and the upstream condition $\phi_i^{(1)} = 0$ when the equations are totally hyperbolic or the condition that $\phi_i^{(1)} = 0$ at $y = \pm\infty$ when the equations are totally elliptic. For systems which are neither totally elliptic nor hyperbolic we employ a suitable combination of the latter two conditions.

b. *Rigid Upper Surface*

The condition that the upper surface remain fixed may be written

$$\sum_{i=0}^{n} h_i = H$$

or in terms of $h_i^{(1)}$

$$\sum_{i=0}^{n} h_i^{(1)} = 0. \tag{10}$$

As the pressure at the fluid top is no longer constant when the upper surface is rigid, we expand p_s in terms of ε

$$p_s = P_s + \varepsilon p_s^{(1)} + \varepsilon^2 p_s^{(2)} + \cdots, \tag{11}$$

where P_s is the upstream value of p_s. Substitution of (6), (7), and (11) into (3) and (4), using the rigid upper surface condition (10), and ignoring $O(\varepsilon^2)$ terms, we obtain

$$H_i \nabla^2 \phi_i^{(1)} + U_i \frac{\partial}{\partial x} h_i^{(1)} = 0, \tag{12}$$

$$U_i \frac{\partial \phi_i^{(1)}}{\partial x} + g \sum_{j=i+1}^{n-1} \frac{\rho_j - \rho_n}{\rho_i} h_j^{(1)} + g \left(1 - \frac{\rho_n}{\rho_i}\right) \sum_{j=0}^{i} h_j^{(1)} + \frac{p_s}{\rho_i} = 0. \tag{13}$$

As in the free upper surface case we eliminate the layer thickness terms in (13) using (12) to obtain a system of equations for the velocity potentials. The general discussion of the method of solution for the n-layer problem with free upper surface also applies here. Thus we present instead explicit results for the simple case of linear two-layer flow with a rigid upper surface. Presentation of this material is relevant to the numerical algorithm for the nonlinear equations proposed in the next section.

We define the nondimensional variables $\mathbf{u}_1'$, $\mathbf{u}_2'$, η, and ζ_0 as

$$\mathbf{u}_i = (u_i, v_i) = U_1 \sqrt{\rho_1/\rho_i}\, \mathbf{u}_i',$$

$$h_0 = H_1 \zeta_0,$$

$$h_1 = H_1(1 - \zeta_0 + \eta).$$

The rigid upper surface condition is

$$h_0 + h_1 + h_2 = H_1 + H_2,$$

which, along with the expressions for h_0 and h_1, implies that

$$h_2 = H_1(\alpha - \eta),$$

where $\alpha = H_2/H_1$. The nonlinear governing equations (3) and (4) in terms of these nondimensional variables take the form

$$(1 + \eta - \zeta_0)\, \nabla \cdot \mathbf{u}_1' + \mathbf{u}_1' \cdot \nabla \eta = \mathbf{u}_1' \cdot \nabla \zeta_0, \tag{14}$$

$$(\alpha - \eta)\, \nabla \cdot \mathbf{u}_2' - \mathbf{u}_2' \cdot \nabla \eta = 0, \tag{15}$$

$$\nabla \times \mathbf{u}_1' = 0, \tag{16}$$

$$\nabla \times \mathbf{u}_2' = 0, \tag{17}$$

$$\eta = F^2(\mathbf{u}_2' - \mathbf{u}_1' + 1 - \beta^2), \tag{18}$$

where we have introduced the parameters

$$F^2 = \frac{U_1^2}{2gH_1} \frac{1}{1 - \rho_2/\rho_1},$$

$$\beta^2 = \left(\frac{U_2}{U_1}\right)^2 \frac{\rho_2}{\rho_1},$$

$$\alpha = \frac{H_2}{H_1}.$$

The Froude number, as defined here for a two-layer system, is the ratio of the bouyancy force to inertia force. Equivalence of F in two-layer flows ensures dynamic similarity.

We note the values of the dependent variables far upstream,

$$\mathbf{u}_2' = (u_2', v_2') = ((U_2/U_1)\sqrt{\rho_2/\rho_1}, 0) = (\beta, 0),$$
$$\mathbf{u}_1' = (u_1', v_1') = (1, 0),$$
$$\eta = 0,$$
$$\zeta_0 = 0.$$

Substitution of the following expansions in terms of ε,

$$\mathbf{u}_2' = \nabla(\beta x + \phi_2) = \nabla(\beta x + \varepsilon\phi_2^{(1)} + \varepsilon^2\phi_2^{(2)} + \cdots),$$
$$\mathbf{u}_1' = \nabla(x + \phi_1) = \nabla(x + \varepsilon\phi_1^{(1)} + \varepsilon^2\phi_1^{(2)} + \cdots),$$
$$\eta = \varepsilon\eta^{(1)} + \varepsilon^2\eta^{(2)} + \cdots,$$
$$\zeta_0 = \varepsilon\zeta_0^{(1)},$$

into (14) through (18) and ignoring $O(\varepsilon^2)$ terms, yields

$$\Phi_{xx}^{(1)} + \Phi_{yy}^{(1)} = \beta\frac{\partial\zeta_0^{(1)}}{\partial x}, \tag{19}$$

$$(1 - M^2)\,\Psi_{xx}^{(1)} + \Psi_{yy}^{(1)} = \frac{\partial\zeta_0^{(1)}}{\partial x}, \tag{20}$$

$$\eta^{(1)} = -2F^2\Psi_x^{(1)}, \tag{21}$$

where

$$\Phi^{(1)} = \beta\phi_1^{(1)} + \alpha\phi_2^{(1)},$$
$$\Psi^{(1)} = \phi_1^{(1)} - \beta\phi_2^{(1)},$$
$$M^2 = 2F^2(1 + (\beta^2/\alpha)).$$

We choose as our obstacle the particularly simple case of a cylinder extending through the total fluid depth and having horizontal cross-section streamlined in the direction of the flow (see Fig. 2). The boundary condition on the vertical cylinder walls is that the component of the fluid velocity normal to the cylinder vanish. To order ε this condition takes the form

$$\Phi_y^{(1)} = \beta(1 + \alpha)\,F'(x) \qquad \text{at} \quad y = 0, \tag{22}$$

$$\Psi_y^{(1)} = (1 - \beta^2)\,F'(x) \qquad \text{at} \quad y = 0. \tag{23}$$

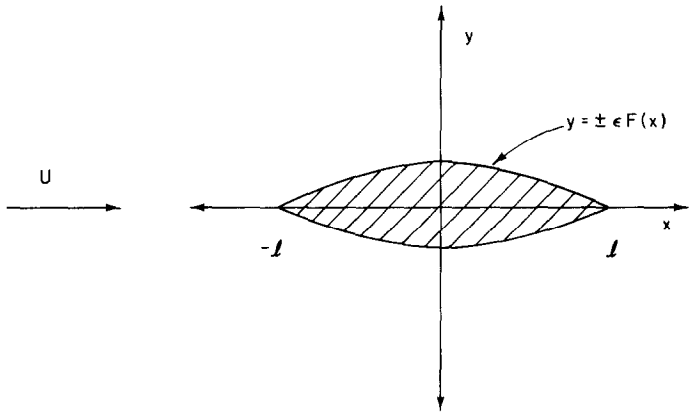

FIG. 2. Flow around a cylinder.

The upstream boundary condition is

$$\Phi^{(1)} = \Psi^{(1)} = 0. \tag{24}$$

Thus the equations governing linear two-layer flow over an obstacle are shown to be in the form of a decoupled pair of second order PDEs given by (19) and (20). (Note that the terms to the right of the equals sign in (19) and (20) vanish for flow past a cylinder.) The solution to (19), (20) satisfying the boundary conditions (22)–(24) is given by

(i) $B = \sqrt{M^2 - 1}$ real,

$$\Phi^{(1)}(x, y) = \frac{\beta(1+\alpha)}{2\pi} \int_{-\infty}^{\infty} F'(\xi) \ln[(\xi - x)^2 + y^2]\, d\xi,$$

$$\Psi^{(1)}(x, y) = \frac{\beta^2 - 1}{B} F(x - By);$$

(ii) $B = \sqrt{M^2 - 1}$ imaginary,

$$\Phi^{(1)}(x, y) = \frac{\beta(1+\alpha)}{2\pi} \int_{-\infty}^{\infty} F'(\xi) \ln[(\xi - x)^2 + y^2]\, d\xi,$$

$$\Psi^{(1)}(x, y) = \frac{1 - \beta^2}{2\pi} \int_{-\infty}^{\infty} F'(\xi) \ln[(\xi - x)^2 + (\mathrm{Re}\, By)^2]\, d\xi.$$

The fundamental difference between these two solutions is characterized by the predicted behavior of the interface between the two fluids. The disturbance on the interface is given by $\eta^{(1)}(x, y)$, which according to (21), depends only on $\Psi^{(1)}$. Thus, for the solution corresponding to real values of B, the interface is disturbed only

along the characteristics ($x - By = \text{const}$) emanating from the cylinder in the downstream direction, while for solutions corresponding to imaginary B, the disturbance is felt throughout the entire flow field. We note also that for general upstream flow speeds, the value of M^2, where

$$M^2 = \left(\frac{U_1^2}{gH_1} + \frac{\rho_2}{\rho_1}\frac{U_2^2}{gH_2}\right)\left(1 - \frac{\rho_2}{\rho_1}\right)^{-1}$$

can always be made arbitrarily large by choosing ρ_2/ρ_1 sufficiently close to unity. Thus, for example, it is possible to produce hypersonic flow phenomena by towing a thin cylinder at an arbitrary slow speed through such a two-layered system so long as ρ_2/ρ_1 is sufficiently close to 1. The system described here is therefore potentially useful as an experimental model for the visualization of hypersonic flow problems.

4. A Numerical Algorithm

In this section we present a numerical algorithm for solving the nonlinear system of equations derived in Section 2. Since standard numerical techniques are readily applicable to this problem when the system of equations is totally hyperbolic or totally elliptic, the proposed algorithm is designed to handle systems of mixed type. For the sake of clarity, we note that the term "mixed type" can refer to different situations. The standard use of this term is in reference to second-order equations which are elliptic in one region but hyperbolic in an adjacent region. A second possibility is in reference to systems of order $n > 2$ for which m characteristic directions are real throughout the flow field and the remaining $n - m$ ($0 < n - m < n$) are imaginary. We restrict our attention to systems of mixed type in the latter sense. An example of such a system of equations is given by the nonlinear equations governing the flow of a two-fluid system with a rigid upper surface. These equations possess one set of characteristics which is always imaginary and a second set which is real for obstacles of moderate size whenever either the upstream flow speeds are sufficiently large or the density ratio ρ_2/ρ_1 is sufficiently close to 1. Similarly, for a two-fluid system with a free upper surface, one finds that the nonlinear equations possess one set of real and one set of imaginary characteristics so long as the density ratio is close to one and the upstream velocities and obstacle heights are moderate. The related phenomena of hydraulic jumps and governing equations of mixed type in the first sense mentioned above presumably occur in flow systems having larger than moderate obstacle heights. These conclusions concerning the characteristics of the two-layer model can be straightforwardly generalized to n-layer models.

The algorithm for the solution of the nonlinear equations will be presented here for the two-layer model. The procedure can in principle be extended for the treatment of many-layered models; each additional layer introduces two new first-order equations specifying the horizontal velocity components in that layer. These equations, as outlined below, are integrated iteratively according to standard methods for hyperbolic or elliptic equations depending on whether the associated characteristics are real or imaginary. The practicality of this method for multilayered models has yet to be

demonstrated, however, since the addition of layers increases the complexity of the algebra required for the determination of the characteristic directions.

The basic steps in the proposed algorithm for the general n-layer model are as follows.

(i) Express the $2n$ equations for the horizontal velocity components (e.g., Eqs. (14)–(17) for a two-layer model) in characteristic form. Corresponding to each characteristic direction $\mathbf{c}_i$ we obtain an equation, referred to as a compatibility relation, containing only differentiations in the direction of $\mathbf{c}_i$.

(ii) Assuming $2r$ real characteristic directions and $2n - 2r$ complex (paired) directions, group into two sets of equations the $2r$ compatibility relations corresponding to the real directions and the $2n - 2r$ relations corresponding to the complex directions.

(iii) Over a suitably chosen mesh in the xy plane make an initial guess of the horizontal velocity components $(u_{i,j}^{(0)}, v_{i,j}^{(0)})$; $i = 1,..., n$; $j = 1,...,$ total number of mesh points.

(iv) Using the compatibility relations corresponding to the real characteristics and standard numerical methods appropriate to hyperbolic equations (e.g., the characteristic method) obtain an improved estimate of $2r$ velocity components.

(v) Using the compatibility relations corresponding to the imaginary characteristics and relaxation techniques, appropriate to elliptic equations, obtain improved estimates of the remaining $2n - 2r$ velocity components.

(vi) Iterate steps (iv) and (v) until, for instance,

$$\max_{\text{all } i,j} |u_{i,j}^{(k+1)} - u_{i,j}^{(k)}| + |v_{i,j}^{(k+1)} - v_{i,j}^{(k)}| < \varepsilon_0,$$

where ε_0 is some suitably chosen convergence criteria.

For the sake of simplicity, we shall illustrate the above computation steps for Eqs. (14)–(18) governing the flow of a two-fluid system bounded above by a flat rigid surface and below by an obstacle whose height vanishes as $|(x, y)| \to \infty$. First, Eqs. (14)–(17) are reduced to characteristic form employing the method of von Mises [9], applicable to a general system of n first-order PDEs. Here we shall briefly illustrate the procedure using the linearized form of Eqs. (14)–(17):

$$(1 - 2F^2)\frac{\partial u_1}{\partial x} + \frac{\partial v_1}{\partial y} + 2F^2\beta\frac{\partial u_2}{\partial x} = \frac{\partial \zeta_0}{\partial x}, \tag{25}$$

$$2F^2\beta\frac{\partial u_1}{\partial x} + (\alpha - 2F^2\beta^2)\frac{\partial u_2}{\partial x} + \alpha\frac{\partial v_2}{\partial y} = 0, \tag{26}$$

$$\frac{\partial u_1}{\partial y} - \frac{\partial v_1}{\partial x} = 0, \tag{27}$$

$$\frac{\partial u_2}{\partial y} - \frac{\partial v_2}{\partial x} = 0. \tag{28}$$

Such a system can be written in vector form as

$$\sum_{j=1}^{n} \mathbf{a}_{ij} \cdot \nabla w_j = b_i, \qquad i = 1,..., n,$$

where, for the above system, $n = 4$, $\mathbf{w} = (u_1, v_1, u_2, v_2)$, the 16 vectors $\mathbf{a}_{ij}$ are

$\mathbf{a}_{11}$:	$(1-2F^2, 0)$	$\mathbf{a}_{12}$:	$(0, 1)$	$\mathbf{a}_{13}$:	$(2F^2\beta, 0)$	$\mathbf{a}_{14}$:	$(0, 0)$
$\mathbf{a}_{21}$:	$(2F^2\beta, 0)$	$\mathbf{a}_{22}$:	$(0, 0)$	$\mathbf{a}_{23}$:	$(\alpha - 2F^2\beta^2, 0)$	$\mathbf{a}_{24}$:	$(0, \alpha)$
$\mathbf{a}_{31}$:	$(0, 1)$	$\mathbf{a}_{32}$:	$(-1, 0)$	$\mathbf{a}_{33}$:	$(0, 0)$	$\mathbf{a}_{34}$:	$(0, 0)$
$\mathbf{a}_{41}$:	$(0, 0)$	$\mathbf{a}_{42}$:	$(0, 0)$	$\mathbf{a}_{43}$:	$(0, 1)$	$\mathbf{a}_{44}$:	$(-1, 0)$

and the 4 components of $\mathbf{b}$ are

$$b_1 = \frac{\partial \zeta_0}{\partial x}, \qquad b_2 = b_3 = b_4 = 0.$$

A necessary condition that the vector $\boldsymbol{\lambda} = (\lambda_1, \lambda_2)$ be normal to a characteristic direction is that the determinant of the matrix $\bar{M}$ with components $M_{ij} = \boldsymbol{\lambda} \cdot \mathbf{a}_{ij}$ be equal to zero; i.e.,

$$\det \bar{M} = 0.$$

For Eqs. (25)–(28) this reduces to

$$[(\lambda_1/\lambda_2)^2 + 1]\{[1 - 2F^2(1 + \beta^2/\alpha)](\lambda_1/\lambda_2)^2 + 1\} = 0.$$

Thus the slopes of the characteristic directions are given by

$$-\lambda_1/\lambda_2 = \pm i, \qquad \pm[2F^2(1 + \beta^2/\alpha) - 1]^{-1/2}.$$

In the remainder of this section we assume that $2F^2(1 + \beta^2/\alpha) > 1$; for the case $2F^2(1 + \beta^2/\alpha) < 1$ the equations are totally elliptic and standard relaxation techniques are applicable. The compatibility relations corresponding to the characteristic directions are obtained by taking suitable linear combinations of Eqs. (25)–(28). The set of four multipliers M_1, M_2, M_3, and M_4 are determined up to a multiplicative constant by the system

$$(1 - 2F^2)\lambda_1 M_1 + 2F^2\beta\lambda_1 M_2 + \lambda_2 M_3 = 0, \tag{29}$$

$$\lambda_2 M_1 - \lambda_1 M_3 = 0, \tag{30}$$

$$2F^2\beta\lambda_1 M_1 + (\alpha - 2F^2\beta^2)\lambda_1 M_2 + \lambda_2 M_4 = 0, \tag{31}$$

$$\alpha\lambda_2 M_2 - \lambda_1 M_4 = 0. \tag{32}$$

A convenient choice of multipliers satisfying (29)–(32) is given by

$$M_1 = -2F^2\beta(\lambda_1/\lambda_2)^3,$$
$$M_2 = (1-2F^2)(\lambda_1/\lambda_2)^3 + (\lambda_1/\lambda_2),$$
$$M_3 = -2F^2\beta(\lambda_1/\lambda_2)^2,$$
$$M_4 = \alpha(1-2F^2)(\lambda_1/\lambda_2)^2 + \alpha.$$

The compatibility relations are then obtained by taking the following linear combinations of Eqs. (25)–(28):

$$M_1\left[(1-2F^2)\frac{\partial u_1}{\partial x} + \frac{\partial v_1}{\partial y} + 2F^2\beta\frac{\partial u_2}{\partial x}\right]$$
$$+ M_2\left[2F^2\beta\frac{\partial u_1}{\partial x} + (\alpha - 2F^2\beta^2)\frac{\partial u_2}{\partial x} + \alpha\frac{\partial v_2}{\partial y}\right]$$
$$+ M_3\left[\frac{\partial u_1}{\partial y} - \frac{\partial v_1}{\partial x}\right] + M_4\left[\frac{\partial u_2}{\partial y} - \frac{\partial v_2}{\partial x}\right] = M_1\frac{\partial \zeta_0}{\partial x}$$

which reduces to

$$\left\{\left[1-2F^2\left(1+\frac{\beta^2}{\alpha}\right)\right]\tan^2\theta + \left(1-2F^2\frac{\beta^2}{\alpha}\right)\right\}\frac{\partial u_2}{\partial \sigma}$$
$$+ \left\{\left[2F^2\left(1+\frac{\beta^2}{\alpha}\right)-1\right]\tan^3\theta + \left(2F^2\frac{\beta^2}{\alpha}-1\right)\tan\theta\right\}\frac{\partial v_2}{\partial \sigma}$$
$$+ \left\{2F^2\frac{\beta}{\alpha}\right\}\frac{\partial u_1}{\partial \sigma} - \left\{2F^2\frac{\beta}{\alpha}\tan\theta\right\}\frac{\partial v_1}{\partial \sigma} = -2F^2\frac{\beta}{\alpha}\frac{\partial \zeta_0}{\partial x}\tan^2\theta, \qquad (33)$$

where $\tan\theta = -\lambda_1/\lambda_2$, so that θ denotes the angle between a characteristic direction and the x axis, and $\partial/\partial\sigma = \partial/\partial x + \tan\theta(\partial/\partial y)$ denotes differentiation along a characteristic. Corresponding to the real directions

$$\tan\theta = \pm\left[2F^2\left(1+\frac{\beta^2}{\alpha}\right)-1\right]^{-1/2},$$

we obtain the relations

$$\frac{\partial}{\partial\sigma}(u_1 - \beta u_2) - \tan\theta\frac{\partial}{\partial\sigma}(v_1 - \beta v_2) = -\tan^2\theta\frac{\partial\zeta_0}{\partial x}, \qquad (34a, b)$$

and corresponding to the imaginary characteristics $\tan\theta = \pm i$, we obtain

$$\left(\frac{\partial}{\partial x} \pm i\frac{\partial}{\partial y}\right)(\beta u_1 + \alpha u_2) \mp i\left(\frac{\partial}{\partial x} \pm i\frac{\partial}{\partial y}\right)(\beta v_1 + \alpha v_2) = \beta\frac{\partial \zeta_0}{\partial x}. \qquad (35a, b)$$

Equations (34a, b) and (35a, b) are simply a restatement of the result obtained in Section 2 that the linearized equations for this two-layer model decouple into a pair of second-order PDEs. Supposing for the moment that the analytic solution given in Section 2 was not known, we could nonetheless obtain an approximate solution by the following straightforward approach. First, notice that Eqs. (34a, b) are simply the characteristic form of Eq. (20). Thus we can immediately integrate these equations numerically using the method of characteristics, obtaining estimates of $u_1 - \beta u_2$ and $v_1 - \beta v_2$. Secondly, Eqs. (35a, b), which may be written in the alternate form

$$\frac{\partial}{\partial x}(\beta u_1 + \alpha u_2) + \frac{\partial}{\partial y}(\beta v_1 + \alpha v_2) = 0 \qquad (36)$$

$$\frac{\partial}{\partial y}(\beta u_1 + \alpha u_2) - \frac{\partial}{\partial x}(\beta v_1 + \alpha v_2) = 0 \qquad (37)$$

are equivalent to Eq. (19), a second-order eliptic PDE. Thus these equations may be integrated numerically using relaxation techniques to obtain estimates of $\beta u_1 + \alpha u_2$ and $\beta v_1 + \alpha v_2$. In the limit of zero forward step size in the integration of (34a, b) and zero mesh width in the integration of (36) and (37), this method is exact. The crux of the proposed algorithm is to extend this numerical idea to the fully nonlinear equations (e.g., Eqs. (14)–(18) for the two-layer model). Since the nonlinear equations do not generally decouple as in the linear case, the extended method is necessarily an iterative one. During each iterative step we integrate the $2r$ real compatibility relations using standard characteristic methods to obtain $2r$ velocity components (or appropriate linear combinations of components) followed by an integration of the $2n - 2r$ imaginary relations using relaxation techniques to determine the remaining $2n - 2r$ velocity components or combinations thereof. The iterations are repeated until convergence is attained. Of course, there is a real question as to whether or not the iterations do in fact converge and a convergence proof is much desired. As is common in most such iterative procedures for nonlinear problems, however, no proof is presently available. Our confidence in the algorithm rests in the fact that it is convergent in the limit of zero obstacle height and in that our efforts to date in using the method to compute two-layer flows over obstacles of height up to approximately $0.45H_1$ have yielded iterations converging to physically reasonable solutions.

In the remainder of this section we supply some of the details concerning the application of this algorithm to the nonlinear equations (14)–(18). First, employing the procedure outlined above for converting a system of PDEs to characteristic form, we find that the characteristic directions λ_1/λ_2 corresponding to these nonlinear equations are given by the roots of the quartic equation

$$[(\lambda_1/\lambda_2)^2 + 1][a(\lambda_1/\lambda_2)^2 + 2b(\lambda_1/\lambda_2) + c] = 0,$$

where

$$a = (\alpha - \eta)\, u_1^2 - \tfrac{1}{2}F^{-2}(1 - \zeta_0 + \eta)(\alpha - \eta) + (1 - \zeta_0 + \eta)\, u_2^2,$$
$$b = (\alpha - \eta)\, u_1 v_1 + (1 - \zeta_0 + \eta)\, u_2 v_2,$$
$$c = (\alpha - \eta)\, v_1^2 - \tfrac{1}{2}F^{-2}(1 - \zeta_0 + \eta)(\alpha - \eta) + (1 - \zeta_0 + \eta)\, v_2^2.$$

Thus the slopes of the characteristic directions are given by

$$\frac{-\lambda_1}{\lambda_2} = \pm i, \qquad \frac{b \pm \sqrt{b^2 - ac}}{a}.$$

The quantity under the radical sign may be written

$$b^2 - ac = M^2 - 1,$$

where

$$M^2 = 2F^2 \frac{u_1^2 + v_1^2}{(1 - \zeta_0 + \eta)} + 2F^2 \frac{u_2^2 + v_2^2}{(\alpha - \eta)} - 4F^{-4} \frac{(u_1 v_2 - u_2 v_1)^2}{(1 - \zeta_0 + \eta)(\alpha - \eta)}.$$

As in the linear ase we assume that M, the local Mach number for this problem, is greater than 1. The compatibility relations have the form

$$\beta_i^{(1)} \frac{\partial u_2}{\partial \sigma_i} + \beta_i^{(2)} \frac{\partial v_2}{\partial \sigma_i} + \beta_i^{(3)} \frac{\partial u_1}{\partial \sigma_i} + \beta_i^{(4)} \frac{\partial v_1}{\partial \sigma_i} = G_i, \qquad i = 1, 2, 3, 4,$$

where $\partial/\partial\sigma_i = \partial/\partial x + \tan\theta_i(\partial/\partial y)$ denotes differentiation along the ith characteristic and the coefficients $\beta_i^{(k)}$ and the nonhomogeneous term G_i are complicated expressions involving u_2, v_2, u_1, v_1, η, α, β, F, $\tan\theta_i$, ζ_0, $\partial\zeta_0/\partial x$, and $\partial\zeta_0/\partial y$. As previously mentioned, these equations are fully coupled so that there is no immediately obvious choice for the velocity components to be computed during the characteristic method integration step or for those to be computed during the relaxation step. Thus, based on the form of the linearized compatibility relations, we simply define

$$(u_h, v_h) = (u_1 - \beta u_2, v_1 - \beta v_2)$$

to be determined during the characteristic method integration step and

$$(u_e, v_e) = (\beta u_1 + \alpha u_2, \beta v_1 + \alpha v_2)$$

to be determined during the relaxation step. In terms of these new variables the two real compatibility relations have the form

$$\beta_\pm^{(1)} \frac{\partial u_h}{\partial \sigma_\pm} + \beta_\pm^{(2)} \frac{\partial v_h}{\partial \sigma_\pm} = -\beta_\pm^{(3)} \frac{\partial u_e}{\partial \sigma_\pm} - \beta_\pm^{(4)} \frac{\partial v_e}{\partial \sigma_\pm} + G_\pm, \qquad \text{(38a, b)}$$

where again $\partial/\partial\sigma_\pm$ denotes differentiation along the real characteristic directions $\tan\theta_\pm$ and the coefficients $\beta_\pm^{(k)}$ and nonhomogeneous terms $G_\pm$ are complicated expressions involving u_h, v_h, u_e, v_e, α, β, η, F, $\tan\theta_\pm$, ζ_0, $\partial\zeta_0/\partial y$, and $\partial\zeta_0/\partial y$. The iterations commence with an initial guess $(u_h^{(0)}, v_h^{(0)}, u_e^{(0)}, v_e^{(0)})$ of (u_h, v_h, u_e, v_e) at the nodal points of a suitable rectangular grid in the horizontal xy plane. Substitution of these values into all terms in Eqs. (38a, b) excepting derivatives appearing on the left-hand sides, we obtain two equations which are integrated stepwise along the two sets of characteristic curves emanating from the upstream boundary according to standard methods. The initial conditions along the upstream boundary and the boundary conditions along the noncharacteristic lines $y=0$ and $y=y_{\max}$ are given schematically in Fig. 3b. The upstream condition is simply that the flow should have the prescribed upstream values $(u_h, v_h)=(1-\beta^2, 0)$ and the boundary $y=0$ is assumed to be a surface of symmetry so that $v_h=0$ there. For the problem of flow past a cylinder symmetric about $y=0$ and extending through the entire fluid depth, we require that the component of (u_h, v_h) normal to the cylinder vanish. We also assume that the mesh encloses a large enough portion of the fow field so that along the boundary $y=y_{\max}$ we may neglect disturbances in the y direction; i.e., we assume $v_h=0$ along this surface. The result of this integration step is a set of values $(u_h^{(1)}, v_h^{(1)})$ defined on the nodal points of the rectangular mesh in the xy plane.

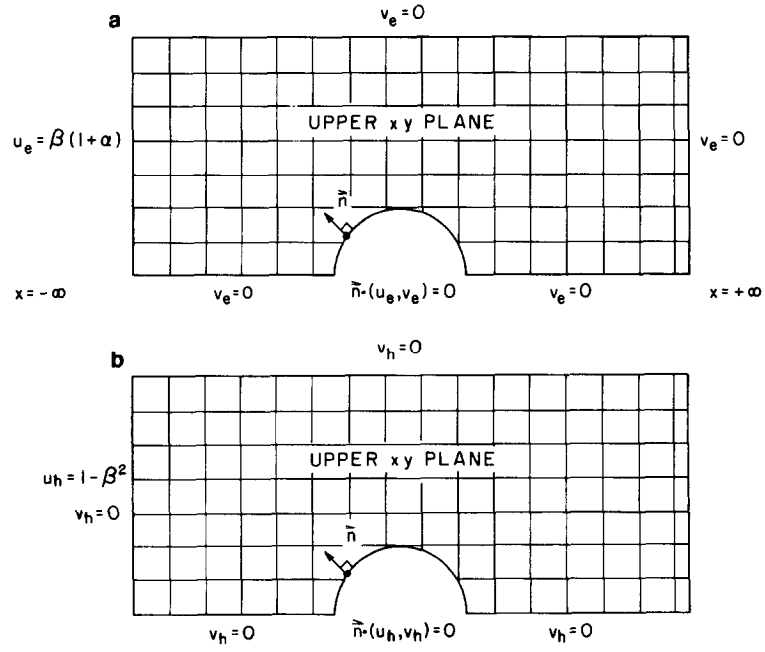

FIG. 3. (a) Boundary conditions for relaxation scheme. (b) Initial and boundary conditions for integration along characteristics. (Letter with overhead arrows in figure are equivalent to boldface letters in text.)

The compatibility relations corresponding to the imaginary characteristics are of the form

$$(\alpha_R^{(1)} \pm i\alpha_I^{(1)}) \left(\frac{\partial u_h}{\partial x} \pm i\frac{\partial u_h}{\partial y}\right) + (\alpha_R^{(2)} \pm i\alpha_I^{(2)}) \left(\frac{\partial u_e}{\partial x} \pm i\frac{\partial u_e}{\partial y}\right)$$
$$+ (\alpha_R^{(3)} \pm i\alpha_I^{(3)}) \left(\frac{\partial v_h}{\partial x} \pm i\frac{\partial v_h}{\partial y}\right) + (\alpha_R^{(4)} \pm i\alpha_I^{(4)}) \left(\frac{\partial v_e}{\partial x} \pm i\frac{\partial v_e}{\partial y}\right)$$
$$= G_R \pm iG_I,$$

where $\alpha_R^{(k)}$, $\alpha_I^{(k)}$, G_R, G_I are complicated real expressions involving u_h, v_h, u_e, v_e, α, β, η, F, ζ_0, $\partial\zeta_0/\partial x$, and $\partial\zeta_0/\partial y$. Addition and subtraction of these two equations yields two real equations which are used to obtain

$$H_{42}\nabla^2 u_e + \nabla H_{42} \cdot \nabla u_e - \hat{k} \times \nabla G_{42} \cdot \nabla u_e$$
$$= -H_{41}\nabla^2 u_h - \nabla H_{41} \cdot \nabla u_h + \hat{k} \times \nabla G_{41} \cdot \nabla u_h - H_{43}\nabla^2 v_h$$
$$- \nabla H_{43} \cdot \nabla v_h + \hat{k} \times \nabla G_{43} \cdot \nabla v_h + \frac{\partial}{\partial x}E_4 - \frac{\partial}{\partial y}F_4 \tag{39}$$

expressing u_e in terms of u_h and v_h, and

$$H_{24}\nabla^2 v_e + \nabla H_{24} \cdot \nabla v_e - \hat{k} \times \nabla G_{24} \cdot \nabla v_e$$
$$= -H_{21}\nabla^2 u_h - \nabla H_{21} \cdot \nabla u_h + \hat{k} \times \nabla G_{21} \cdot \nabla u_h - H_{23}\nabla^2 v_h$$
$$- \nabla H_{23} \cdot \nabla v_h + \hat{k} \times \nabla G_{23} \cdot \nabla v_h + \frac{\partial}{\partial x}E_2 - \frac{\partial}{\partial y}F_2 \tag{40}$$

expressing v_e in terms of u_h and v_h, where

$$G_{ij} = \frac{\alpha_R^{(i)}\alpha_R^{(j)} + \alpha_I^{(i)}\alpha_I^{(j)}}{\alpha_R^{(i)2} + \alpha_I^{(i)2}}, \qquad H_{ij} = \frac{\alpha_R^{(i)}\alpha_I^{(j)} - \alpha_I^{(i)}\alpha_R^{(j)}}{\alpha_R^{(i)2} + \alpha_I^{(i)2}},$$
$$E_i = \frac{\alpha_R^{(i)}G_I - \alpha_I^{(i)}G_R}{\alpha_R^{(i)2} + \alpha_I^{(i)2}}, \qquad F_i = \frac{\alpha_R^{(i)}G_R + \alpha_I^{(i)}G_I}{\alpha_R^{(i)2} + \alpha_I^{(i)2}},$$

and $\hat{k}$ is the unit vector in the vertical z direction. All derivatives in (39) and (40) are replaced with central difference approximations, the velocity components (u_h, v_h) are replaced with $(u_h^{(1)}, v_h^{(1)})$ and velocity components (u_e, v_e) are replaced with the initial guesses $(u_e^{(0)}, v_e^{(0)})$ everywhere except in the derivatives appearing on the left-hand sides of the equations. Integration by standard relaxation techniques yields the improved estimates $(u_e^{(1)}, v_e^{(1)})$. The boundary conditions employed in this procedure are given schematically in Fig. 3a. On the upstream boundary we assume $(u_1, v_1) = (1, 0)$ and $(u_2, v_2) = (\beta, 0)$ which gives the condition $u_e = \beta(1 + \alpha)$. On the boundary $y = 0$, which is assumed here to be a surface of symmetry, we have $v_e = 0$. We also

assume that the mesh encloses a large enough portion of the flow field so that on the boundaries furthest from the obstacle in the positive y and downstream directions, we may neglect any disturbances in the y direction. Again for flow around a cylinder one must require that the component of (u_e, v_e) normal to the cylinder vanish.

Repeated iterations of this scheme result in successive approximations $(u_h^{(k)}, v_h^{(k)}, u_e^{(k)}, v_e^{(k)})$ which hopefully converge to a physically reasonable solution. As previously stated, our experience with the algorithm has indicated that the iterations do in fact converge so long as the obstacle heights are moderate and the relevant flow parameters fall within certain bounds. Examples of our calculations are presented in the next section.

5. Results

The algorithm described in Section 4 has been applied to the problem of two-layer flow over various types of obstacles. Calculations have been performed for both free upper surface and rigid upper surface flows. Three cases are presented.

c. Flow past a Cylinder: Rigid Upper Surface

cylinder. The upper boundary of the flow is taken to be a rigid horizontal surface. The flow is left to right and the values of the relevant paremeters are $F^2 = 1.2$, $\alpha = 1.0$, $\beta = 0.75$, and $\gamma = 0.237$. Here we define γ to be the cylinder width in the direction perpendicular to the flow divided by its length flowwise. Comparison of such solutions corresponding to small γ agree well with the linear solutions (obtained

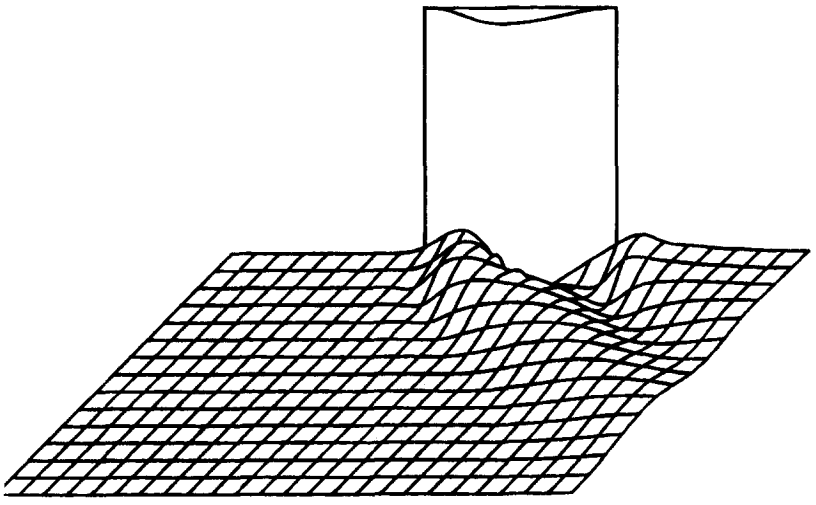

FIG. 4. Flow past a cylinder; $F^2 = 1.2$, $\alpha = 1.0$, $\beta = 0.75$, $\gamma = 0.237$.

in Section 3) in the region adjacent to or just downstream of the cylinder. Further downstream of the obstacle, nonlinear effects are important even for small γ. An important question concerning such solutions is whether or not continuous solutions truly exist. For example, for the related problem of the supersonic flow of a compressible gas around a wedge, shocks are known to extend downstream from the leading edge. However, the equations governing two-layered flow are partially elliptic in nature owing to the set of imaginary characteristics. This feature of the two-layer model equations is illustrated in Fig. 5. Here we plot the two families of characteristic curves in the upper xy plane. The flow again is left to right. The dashed lines have the slope of the characteristics far upstream. Important here are the characteristics just upstream of the leading edge of the cylinder. Due to the elliptic nature of the equations, effects of the disturbance have propagated upstream, with the result that each of the families of characteristic curves fill the entire flow region in such a way that no two curves intersect. In contrast, the characteristics for the supersonic flow of a compressible gas around a thin wedge cross each other along a line extending downstream from the leading edge. Such lines of intersecting characteristics reflect the presence of discontinuities or shock waves in the flow, while the absence of intersecting characteristics implies continuous flow. Hence, based on this graphically compelling evidence, we conclude that continuous flows exist for sufficiently small γ. Increasing γ results in solutions whose characteristics become increasingly concentrated near the leading and trailing edges of the cylinder. For larger still γ, continuous flows are no longer possible and a valid theory must allow for the presence of shock waves or hydraulic jumps. The analysis of flows containing such discontinuities is beyond the scope of the present report.

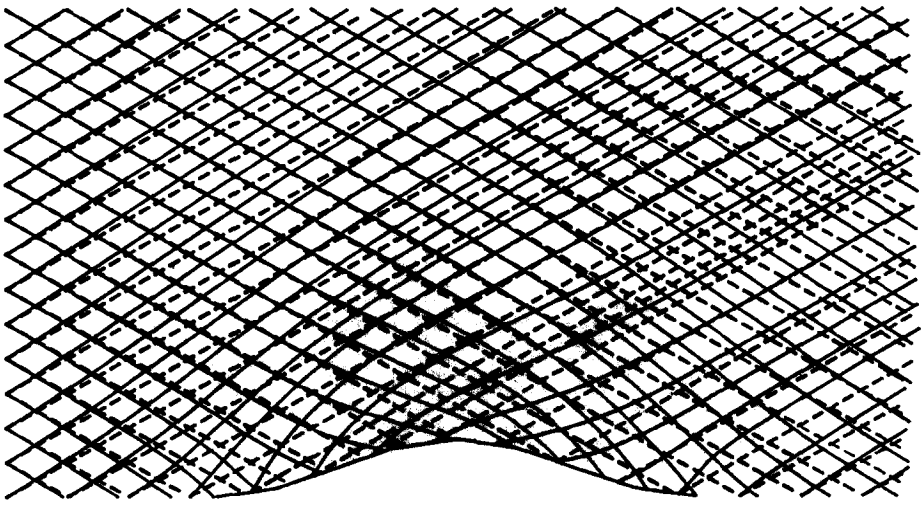

FIG. 5. Characteristics for flow past a cylinder; $F^2 = 1.2$, $\alpha = 1.0$, $\beta = 0.75$, $\gamma = 0.237$.

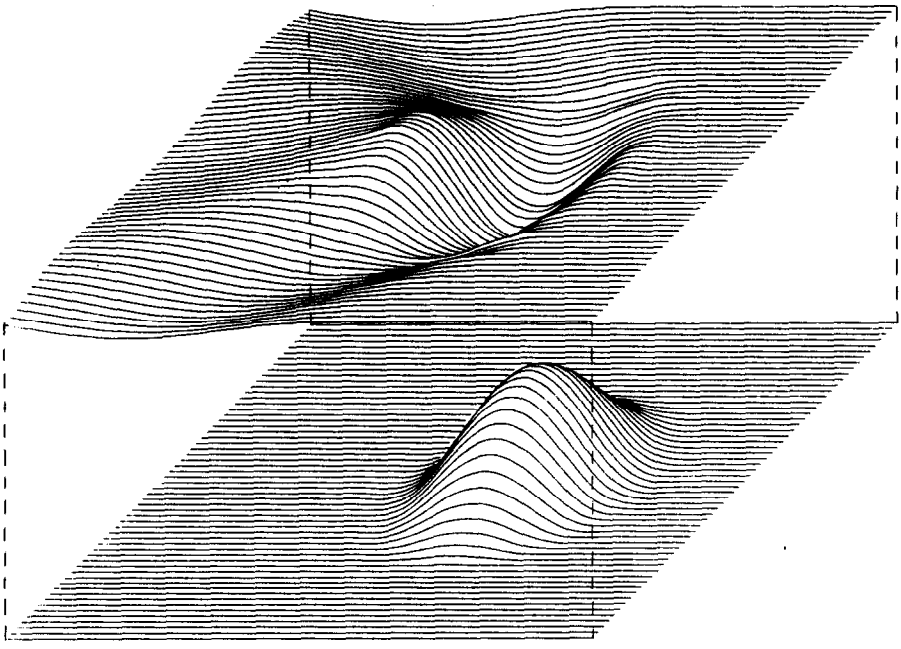

FIG. 6. Flow over a hill; $F^2 = 1.2$, $\alpha = 1.0$, $\beta = 0.75$, $\xi = 0.35$.

b. *Two-layer Flow over an Obstacle; Rigid Upper Surface*

In Fig. 6 we show the interface separating the two fluids for flow over an obstacle on the bottom horizontal surface. The obstacle is pictured below. The flow here is right to left and the values of the relevant parameters are $F^2 = 1.2$, $\alpha = 1.0$, $\beta = 0.75$, and $\xi = 0.35$. The parameter ξ is defined to be the maximum height of the obstacle divided by the upstream thickness of the bottom fluid H_1. We note the following prominent features of the flow. First, the interface is depressed immediately above the obstacle and in a wedge extending downstream of the obstacle. Also, a rise in the interface appears just downstream of the vertex of the wedge followed by a less noticeable depression. Examination of the characteristics reveal that these solutions are continuous and indeed continuous solutions for this obstacle exist for values of ξ up to approximately 0.5. Continuous solutions for larger values of ξ are possible so long as the slope of the obstacle is made more gradual.

c. *Two-layer Flow around an Obstacle Interior to a Layer; Free Upper Surface*

In this case we consider a two-layer fluid model with a obstacle placed interior to one of the layers and a free upper surface (see Fig. 7). The equations governing the flow around an obstacle interior to the bottom layer are identical to those for two-layer flow over an obstacle on the bottom horizontal surface. This is due to the assumption of hydrostatics and the vertical averaging employed in each layer. The

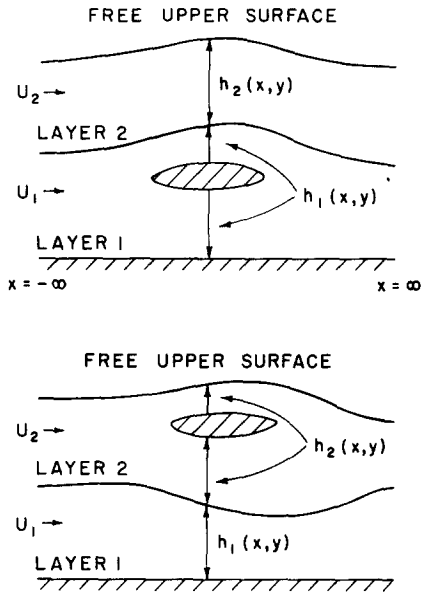

FIG. 7. Schematic of flow around an obstacle interior to a fluid layer.

equations for flow around an obstacle in the upper layer are a straight forward extension of those for flow over an obstacle in the lower layer (see Appendix for details). In Fig. 8 we show the upper surface and interface between the two fluids for flow around an obstacle in the upper layer. The obstacle thickness employed in this calculation, as a function of x and y, is the same as that for the obstacle pictured in Fig. 6 with $\xi = 0.4$. The values of the other relevant parameters are $F^2 = 1.2$, $\alpha = 1.0$, and $\beta = 0.75$. We see that the interface between the two fluid layers is depressed immediately below the obstacle and in a wedge extending downstream, with an accompanying rise just downstream of the vertex of the wedge followed by a slight depression. The disturbance on the top surface has the structure of alternating rises and depressions in the flow direction; the first being a depression just downstream of the obstacle. In Fig. 9 we show the upper surface and interface for flow around the same obstacle employed in the calculations generating Fig. 8; however, this time placed in the lower layer. Again the values of the flow parameters are given by $F^2 = 1.2$, $\alpha = 1.0$, and $\beta = 0.75$. The main feature of the flow pictured here is a prominent rise in the interface separating the two fluids directly above the obstacle with less prominent rises along a wedge extending downstream. On the upper surface the disturbance is qualitatively similar to that for flow around an obstacle in the upper layer (see Fig. 8). We note, however, that at least for this particular set of parameters, the disturbance on the free upper surface is more pronounced for flow around an obstacle in the lower layer than that produced by flow around the same obstacle in the upper layer.

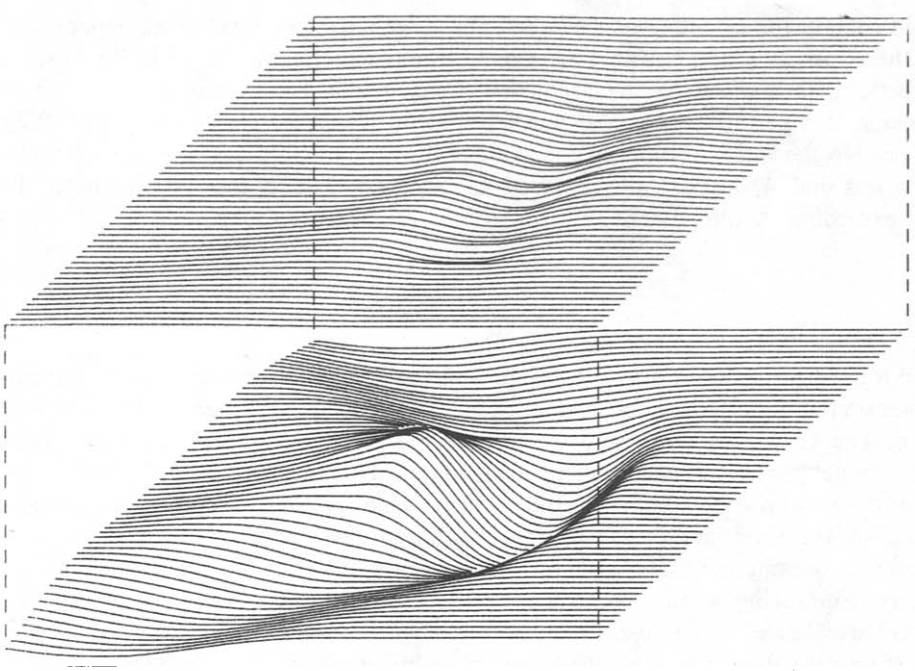

FIG. 8. Flow around an obstacle in upper layer; $F^2 = 1.2$, $\alpha = 1.0$, $\beta = 0.75$, $\xi = 0.4$.

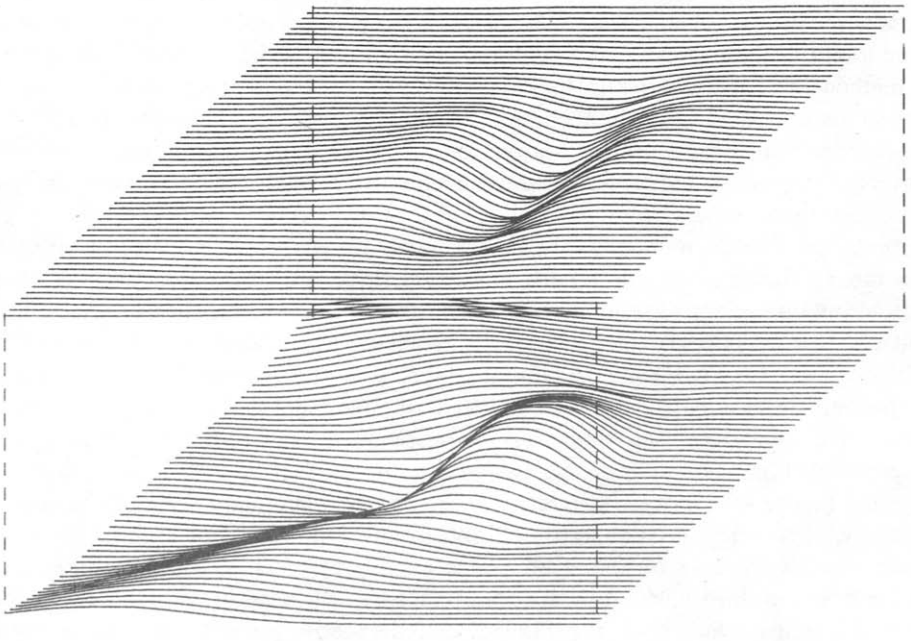

FIG. 9. Flow around an obstable in lower layer; $F^2 = 1.2$, $\alpha = 1.0$, $\beta = 0.75$, $\xi = 0.4$.

In each of the calculations described above we have employed an equispaced mesh in the upper $\frac{1}{2}$ plane having 25 elements in the x direction and 15 in the positive y direction. Each of the obstacles occupied the middle 8 elements along the x axis. Calculations performed on finer meshes confirmed that this mesh size was sufficient to resolve the main features of the various flows. Typically convergence (defined to be a less than 1% error) was achieved in less than 10 iterations with computer times not exceeding 10 min.

6. Discussion

We have presented a numerical algorithm for the nonlinear problem of the three-dimensional, steady flow of a continuously stratified, incompressible, hydrostatic fluid. The key features of the proposed method are as follows. First, we consider a fluid model comprised of n homogeneous layers. This idealization may be thought of as either an approximation to a continuously stratified fluid or alternately one might think of the fluid interfaces separating adjacent layers as approximations to the common oceanic and atmospheric phenomenon of strong temperature inversion layers. Employing vertical averages of the horizontal velocity components in each layer, we derive a nonlinear system of partial differential equations of order $2n$ governing the flow. For most problems of practical interest, this system of equations is of mixed type in the sense described in Section 4. Restricting our attention to this mixed case, we show that the problem may be thought of as a mixed initial value and boundary value problem. That is, we alternately apply relaxation techniques to the compatibility relations associated with the complex characteristics and an integration by method of characteristics to the compatibility relations corresponding to the real characteristics. As outlined in Section 5, we have applied this method to the flow of a two-layered fluid model around various obstacles. The iterations in each case have converged to physically reasonable solutions for values of the model parameters lying within certain bounds.

For larger Froude number flows or for larger or less gradually sloped obstacles than those considered in this report, the actual flows are likely to be discontinuous and/or contain regions of separated flow. To see this consider the flow of a multilayer fluid about a cylinder extending vertically from the lower solid surface $z = 0$ to the fluid top $z = \sum_{i=0}^{n} h_i$. Recall that in each layer only the average horizontal velocity components are computed. For single-layer flow, one has the classical shallow water theory and the governing equations correspond to those for the steady two-dimensional flow of a compressible gas with γ, the ratio of specific heats, equal to 2. Thus the theory of one-layer supercritical flow is completely analogous to the theory of steady, two-dimensional supersonic flows in gas dynamics. For example, then, we expect that in the case of one-layer flow around a cylinder whose horizontal cross section is streamlined in the flow direction, the flow will contain an attached, oblique hydraulic jump while less streamlined cylinders will generate hydraulic jumps detached from the cylinder. For a multilayer model we have in each layer the two-

dimensional flow of a homogeneous fluid about a body defined by the cross section of the cylinder. The main complicating factor is the coupling that exists between different layers. This coupling allows for continuous solutions in the case of very thin cylinders (e.g., results pictured in Figs. 4 and 5); however, for the reasons outlined above we expect that there is a critical thickness (holding fixed the other flow parameters) beyond which continuous solutions do not exist. One plan to extend the algorithm to these discontinuous flows is to apply the extensive existing collection of numerical studies on two-dimensional oblique, attached and detached shock waves in gas dynamics to this problem. This approach seems promising and is the subject of current study.

Another possible extension of this algorithm is to three-dimensional stratified flows over topography in a rotating system. The addition of rotational effects would make the model valid for the study of a wide range of large-scale geophysical problems (e.g., ocean currents around islands or sea mounts, air flow over mountain ranges, Jupiter's Great Red Spot, and interactions between the Earth's liquid core and solid mantle). A particularly promising application of the model appears to be the study of large-scale inertial flows, i.e., flows corresponding to Rossby numbers of order of magnitude 1. It is known, for instance, that the Rossby number for westerm boundary currents in the oceans is typically near unity. Consequently, the large literature of theoretical quasi-geostrophic studies are generally not applicable to these inertial boundary currents. The equations governing the steady three-dimensional flow of an n-layer fluid system on a beta-plane are given by:

(i) continuity or mass conservation equation,

$$\frac{\partial h_i}{\partial t} + \frac{\partial}{\partial x}(h_i \bar{u}_i) + \frac{\partial}{\partial y}(h_i \bar{v}_i) = 0;$$

(ii) Bernoulli's theorem,

$$\frac{D}{Dt}\frac{1}{2}(\bar{u}_i^2 + \bar{v}_i^2) + p_s + g \sum_{j=i+1}^{n} \rho_j h_j + g\rho_i \sum_{j=0}^{i} h_j = 0;$$

(iii) Vorticity equation,

$$\frac{D}{Dt}\frac{\bar{w}_i + f_0 + \beta y}{h_i} = 0,$$

where $\bar{w}_i = \partial \bar{v}_i/\partial x - \partial \bar{u}_i/\partial y$ and $D/Dt = \partial/\partial t + (\bar{u}_i, \bar{v}_i) \cdot \nabla$. Also, the Coriolis parameter $f(y)$ is given by

$$f(y) = f(0) + \beta y = f_0 + \beta y,$$

where $f_0 = 2\Omega \cos \Theta_0$, Ω is the rotation rate of the earth, Θ_0 the latitude

corresponding to $y = 0$, $\beta = 2\Omega \sin \Theta_0/R$ and R is the radius of the earth. The vorticity equation can be integrated to yield

$$\frac{\bar{w}_i + f_0 + \beta y}{h_i} = \frac{-U_i'(Y_i) + f_0 + \beta Y_i}{H_i}$$

for upstream velocity distributions of the form $(U_i(y), 0)$, upstream layer thicknesses H_i, and $Y_i = Y_i(x, y)$ defined to be the upstream y component of the streamline in the ith layer passing through a downstream position (x, y). Note that for upstream horizontal shear of the form

$$U_i'(y) = f_0 + \beta y,$$

the integrated vorticity equation has the particularly simple form

$$\bar{w}_i + f_0 + \beta y = 0.$$

The full set of $3n$ equations for an n-layer model is in the form of a coupled, nonlinear system of first-order PDEs. Our algorithm for nonrotating systems readily extends to this case.

Finally it should be noted that the proposed algorithm, in its present form, can handle only obstacles which either project through the entire fluid depth (i.e., flow around a cylinder) or are contained entirely in a single layer. The more complicated problem of an obstacle projecting through several (but not all) layers is beyond the scope of this paper. As demonstrated by the results presented in this report and as indicated by the above discussion, however, the method is nonetheless potentially capable of handling a wide range of topographic profiles (including detailed realistic profiles of particular mountain ranges or islands) and flow parameters. We feel, therefore, that this procedure has the potential to be an important tool for understanding atmospheric and oceanic phenomena.

APPENDIX: Free Upper Surface Flow around an Interior Obstacle

Here we present the equations governing the steady flow of an n-layer fluid model with a free upper surface and an obstacle interior to the kth layer. The obstacle thickness as a function of x and y is given by $h_0(x, y)$.

In each layer we have the continuity equations and Bernoulli's theorem:

$$\frac{\partial}{\partial x}(h_i u_i) + \frac{\partial}{\partial y}(h_i v_i) = 0,$$

$$\frac{1}{2}(u_i^2 + v_i^2) + p_i = B_i, \qquad i = 1,..., n,$$

where p_i is given by

$$p_i = g \sum_{j=i+1}^{n} \frac{\rho_j}{\rho_i} h_j + g \frac{\rho_k}{\rho_i} h_0 + g \sum_{j=1}^{i} h_j, \qquad k > i,$$

$$= g \sum_{j=i+1}^{n} \frac{\rho_j}{\rho_i} h_j + g \sum_{j=0}^{i} h_j, \qquad k \leqslant i,$$

and the Bernoulli constant B_i is given by

$$B_i = \frac{1}{2} U_i^2 + g \sum_{j=i+1}^{n} \frac{\rho_j}{\rho_i} H_j + g \sum_{j=1}^{i} H_j.$$

The pressure in the ith layer, as a function of x, y, and z, is given by

$$p(x, y, z) = p_s + g \sum_{j=i+1}^{n} \rho_j h_j + g\rho_k h_0 + g\rho_i \left(\sum_{j=1}^{i} h_j - z \right), \qquad k > i,$$

$$= p_s + g \sum_{j=i+1}^{n} \rho_j h_j + g\rho_i \left(\sum_{j=0}^{i} h_j - z \right), \qquad k \leqslant i,$$

where p_s is the (constant) pressure at the fluid top.

For two-layer flow, Bernoulli's theorem for each layer reduces to one of the two following forms, depending on the location of the obstacle:

(a) obstacle in the top layer,

$$\tfrac{1}{2}(u_2^2 + v_2^2) + g(h_0 + h_1 + h_2) = B_2,$$
$$\tfrac{1}{2}(u_1^2 + v_1^2) + g(\rho_2/\rho_1)(h_0 + h_2) + gh_1 = B_1;$$

(b) obstacle in bottom layer,

$$\tfrac{1}{2}(u_2^2 + v_2^2) + g(h_0 + h_1 + h_2) = B_2,$$
$$\tfrac{1}{2}(u_1^2 + v_1^2) + g(\rho_2/\rho_1)\, h_2 + g(h_0 + h_1) = B_1.$$

ACKNOWLEDGMENT

This work was supported by Fluid Dynamics Program of the Office of Naval Research, U. S. Navy.

REFERENCES

1. P. W. M. BRIGHTON, *Quart. J. Roy. Met. Soc.* **104** (1978), 289–307.
2. G. D. CRAPPER, *J. Fluid Mech.* **6** (1959), 51–76.
3. P. G. DRAZIN, *Tellus* **8** (1961), 239–251.
4. J. C. R. HUNT AND W. H. SNYDER, *J. Fluid Mech.* **96** (1980), 671–704.

5. J. D. LEE AND C. H. SU, *J. Geophys. Res.* **82** (1977), 420–426.
6. J. J. RILEY, H. T. LIU, AND E. W. GELLER, "A Numerical and Experimental Study of Stably Stratified Flow around Complex Terrain," U. S. Environ Monitoring Ser. Rep. EPA–600/4 – 76–021, Research Triangle Park, N. C., 1976.
7. W. K. STEVENS, "Two Numerical Methods for Steady Stratified Flows over an Obstacle," Ph.D. thesis, Brown Univ. Division of Applied Mathematics, 1979.
8. C. H. SU, *J. Fluid Mech.* **73** (1976), 33–47.
9. R. VON MISES, "Mathematical Theory of Compressible Fluid Flow," p. 103, Academic Press, New York, 1958.
10. K. K. WONG, *J. Atmos. Sci.* **24** (1972), 1223–1229.